

The Modulo Radon Transform and its Inversion

Ayush Bhandari
Dept. of EE Engineering
Imperial College London
London, SW72AZ, UK.
a.bhandari@imperial.ac.uk

Matthias Beckmann
Dept. of Mathematics
University of Hamburg
Bundesstraße 55, 20146 Hamburg.
matthias.beckmann@uni-hamburg.de

Felix Kraemer
Dept. of Mathematics
Technical University of Munich
Garching 85747, Germany.
felix.kraemer@tum.de

Abstract—In this paper, we introduce the Modulo Radon Transform (MRT) which is complemented by an inversion algorithm. The MRT generalizes the conventional Radon Transform and is obtained via computing modulo of the line integral of a two-dimensional function at a given angle. Since the modulo operation has an aliasing effect on the range of a function, the recorded MRT sinograms are always bounded, thus avoiding information loss arising from saturation or clipping effects. This paves a new pathway for imaging applications such as high dynamic range tomography, a topic that is in its early stages of development. By capitalizing on the recent results on Unlimited Sensing architecture, we prove that the Modulo Radon Transform can be inverted when the resultant (discrete/continuous) measurements map to a band-limited function. Thus, the MRT leads to new possibilities for both conceptualization of inversion algorithms as well as development of new hardware, for instance, for single-shot high dynamic range tomography.

Index Terms—Computational imaging, computer tomography, filtered back projection, modulo, sampling and Radon transform.

I. INTRODUCTION

X-ray imaging, Computed Tomography (CT) and Q-Ball imaging are examples of revolutionary scientific and medical imaging technologies. Many of these methods trace their roots back to the beginning of the 20th century; an era that saw many exciting breakthroughs. In 1901, Röntgen was awarded the Nobel Prize in physics for discovering what is today known as the *X-rays*. In the area of mathematics, in 1904, Minkowski posed the problem of recovering an even function on a sphere, given its integrals over “big circles”. In 1915, Funk [1] solved this problem by providing an explicit formula. In 1917, Radon [2] posed a similar problem based on line integrals in Euclidean spaces. These interdisciplinary ideas culminated into a number of applications with Radon Transform based *computed tomography* (in radiology [3]) being a notable example.

Beyond its applications that have done wonders in medical imaging, the Radon Transform has also been theoretically studied in various fields due to its fundamental significance as a mathematical tool. For instance, it is closely tied to the study of partial differential equations [4]. In signal processing, sampling of the Radon Transform has been considered [5] and discrete versions have been proposed along with fast and efficient recovery algorithms [6]. Finally, in the context of

tomography and integral geometry, some generalizations have been defined, such as the Exponential Radon Transform [7].

Recent Development of High Dynamic Range Tomography.

Our work is motivated by a practical challenge. All modern imaging sensors are based on digital representation of data. In this context, the dynamic range of the sensor recording intensity (or line integral at a given projection angle) is fixed by design. Recent technological advances have led to X-ray sources that are getting more powerful. To leverage from this progress, the detectors as well as the reconstruction algorithms must also be enhanced. A particular challenge to this end is to be able to record high intensity projections. Whenever the intensity of the X-rays traversing a path exceeds the imaging sensor’s threshold, the resultant CT information is lost due to saturation and clipping. To overcome the dynamic range hurdle, a number of papers in the recent years have proposed the idea of exploiting multiple exposures. In [8], Chen et al. propose a new method whereby, at each projection angle, the voltage is adjusted several times (multiple exposures) and this results in measurements corresponding to different intensities. Thereon, a high dynamic range (HDR) image is recovered using image fusion. This approach is known as HDR-CT. In [9], Li et al. automate the approach reported in [8] so that the intensity is self-adapted for HDR imaging. Eppenberger et al. [10] proposed one of the first methods for 32-bit, colored HDR X-ray imaging (cf. Fig. 2, [10]). Their approach utilized an underexposed, an intermediate, and an overexposed image. Multiple-exposure-based HDR imaging has also found applications in fluorescence [11] and ultrasound [12]. Hardware-only approaches have also been recently explored for HDR X-ray imaging. In [13], Weiss et al. propose a method for increasing the sensor’s dynamic range.

Our Contributions. To overcome the dynamic range barrier, in this paper, we take a *single-shot* computational sensing approach that is based on a co-design of hardware and algorithms and avoids multiple exposures. To this end, we propose the *Modulo Radon Transform* (MRT)—a generalization of the conventional Radon Transform—that records the modulo of the Radon Transform. Our work is inspired by the **Unlimited Sensing Architecture** [14]–[16] and exploits the idea that modulo non-linearity folds the amplitudes. Hence, even though the Radon Transform may take arbitrarily large values, the modulo output has a fixed range; this is demonstrated in Fig. 2.

This work was supported by the UK Research and Innovation council’s Future Leaders Fellowship program “Sensing Beyond Barriers” (MRC Fellowship award no. MR/S034897/1).

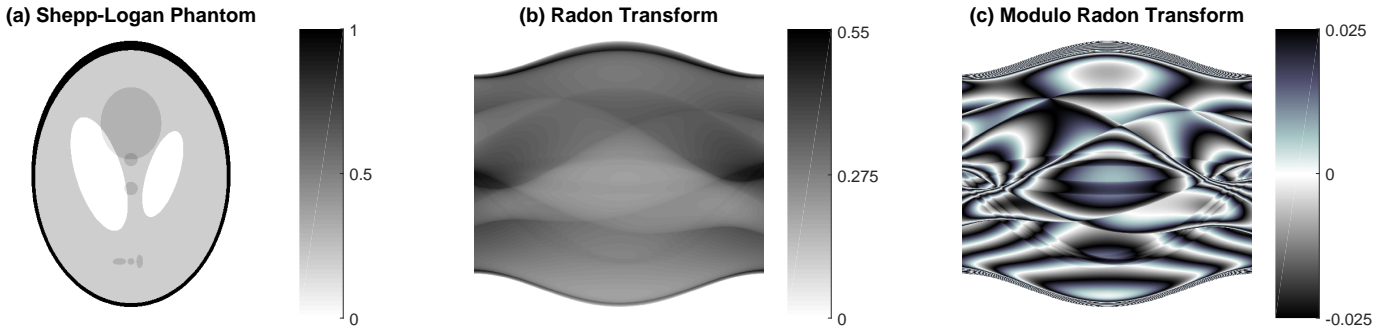


Fig. 1. The Modulo Radon Transform converts high dynamic range tomographic information into low dynamic range samples. (a) The Shepp-Logan phantom. (b) Conventional Radon Transform and (c) Modulo Radon Transform with $\lambda = 0.025$ leading to about a factor of 10-times compression in dynamic range.

Our specific contributions regarding the MRT are as follows:

- We introduce the MRT for integrable functions.
- We take a first step towards the inversion of the MRT and show its injectivity for band-limited functions.
- Our approach is constructive and our mathematical theory is complemented by a recovery algorithm for discrete data that is empirically stable with respect to noise.
- We derive L^2 -error estimates for the reconstruction error in the case of semi-discrete MRT samples of functions from Sobolev spaces of fractional order.

A related problem to our work is that of *phase-unwrapping*. However, controlling redundancy in the acquisition process and resulting recovery guarantees and algorithms is where our approach differs from phase-unwrapping. For more discussion, we refer to [15] and Section V on numerical demonstration.

A Note on Practical Feasibility. We remark that the idea of folding was implicitly realized in the imaging hardware literature (cf. Fast ADCs [17] and reset-ADCs for HDR imaging [18]), however, its link with modulo operator and the resulting inverse problem was never studied. A first step towards this direction was taken in [14]. For detailed overview of related hardware, we refer the reader to [15]. Recently, HDR X-ray imaging using pixel-level customization was discussed in [13]. Since amplitude-folding has already been established in the context of CMOS imagers [14], [15], [18], over time, the folding strategy could certainly be combined with detector technology used in tomography hardware [13].

II. CONVENTIONAL RADON TRANSFORM

Let $f \equiv f(\mathbf{x})$ be the two-dimensional function or image in our setup with spatial coordinates $\mathbf{x} = (x_1, x_2)^\top \in \mathbb{R}^2$. The conventional Radon Transform \mathcal{R} is a mapping of the form

$$\mathcal{R}f(\boldsymbol{\theta}, t) = \int_{\mathbb{R}^2} f(\mathbf{x}) \delta(t - \mathbf{x}^\top \boldsymbol{\theta}) d\mathbf{x} = \int_{\ell_{t, \boldsymbol{\theta}}} f(\mathbf{x}) d\mathbf{x}$$

and computes the line integral along the line $\ell_{t, \boldsymbol{\theta}}$ specified in Hesse normal form by $\mathbf{x}^\top \boldsymbol{\theta} = t$, i.e. $x_1 \cos(\theta) + x_2 \sin(\theta) = t$, where $\boldsymbol{\theta} = (\cos(\theta), \sin(\theta))^\top \in \mathbb{S}^1$ is the projection direction with angle $\theta \in [0, 2\pi)$ and $t \in \mathbb{R}$ is the (signed) distance from the origin. For the sake of brevity, for fixed $\theta \in [0, 2\pi)$ we set

$$\mathcal{R}_\theta f = \mathcal{R}f(\boldsymbol{\theta}, \cdot).$$

It is well-known that $\mathcal{R} : L^1(\mathbb{R}^2) \rightarrow L^1(\mathbb{S}^1 \times \mathbb{R})$ defines a continuous linear operator and the Fourier slice theorem states

$$\mathcal{F}_1(\mathcal{R}_\theta f)(t) = \mathcal{F}_2 f(t\boldsymbol{\theta}) \quad (1)$$

with the d -dimensional Fourier transform

$$\mathcal{F}_d \Phi(\boldsymbol{\omega}) = \int_{\mathbb{R}^d} \Phi(\mathbf{y}) e^{-i\boldsymbol{\omega}^\top \mathbf{y}} d\mathbf{y}.$$

This implies that \mathcal{R} is injective on $L^1(\mathbb{R}^2)$. Under additional assumptions, e.g. $f \in \mathcal{C}_c^\infty(\mathbb{R}^2)$ or $f \in \mathcal{S}(\mathbb{R}^2)$, the inversion of \mathcal{R} is given by the filtered back projection (FBP) formula

$$f(\mathbf{x}) = \frac{1}{2} \mathcal{R}^\# (\mathcal{F}_1^{-1} [|S| \mathcal{F}_1(\mathcal{R}_\theta f)(S)]) (\mathbf{x}),$$

where the back projection $\mathcal{R}^\#$ denotes the rescaled L^2 -adjoint of \mathcal{R} , for $g \equiv g(\boldsymbol{\theta}, t)$ given by

$$\mathcal{R}^\# g(\mathbf{x}) = \frac{1}{2\pi} \int_{\mathbb{S}^1} g(\boldsymbol{\theta}, \mathbf{x}^\top \boldsymbol{\theta}) d\boldsymbol{\theta}.$$

The inversion of \mathcal{R} is a (mildly) ill-posed problem and a common regularization strategy is to choose a band-limited reconstruction filter $F_\Omega \in \text{PW}_\Omega$ with bandwidth $\Omega > 0$ and apply the approximate FBP reconstruction formula

$$f_\Omega = \frac{1}{2} \mathcal{R}^\# (F_\Omega * \mathcal{R}_\theta f). \quad (2)$$

The influence of F_Ω on the approximation quality of f_Ω in Sobolev spaces of fractional order is analysed in [19]–[21].

The Radon Transform measurements are converted to a discrete-time form via generalized sampling operation yielding the projections

$$p_\theta[m] = \int_{\mathbb{R}} \mathcal{R}_\theta f(t) \phi(mT - t) dt = p_\theta(mT). \quad (3)$$

Here T is the sampling rate of the kernel $\phi \in L^2(\mathbb{R})$ which characterizes the impulse response of the detector used for data acquisition. Note that $\{\ell_{mT, \boldsymbol{\theta}}\}_{m \in \mathbb{Z}}$ defines a family of parallel lines with fixed direction $\boldsymbol{\theta} \in \mathbb{S}^1$. This setup is used in what is known as parallel beam geometry. As \mathcal{R} satisfies the evenness condition

$$\mathcal{R}f(-\boldsymbol{\theta}, -t) = \mathcal{R}f(\boldsymbol{\theta}, t) \quad \forall (\boldsymbol{\theta}, t) \in \mathbb{S}^1 \times \mathbb{R},$$

it suffices to collect the data at projection angles $\theta \in [0, \pi)$.

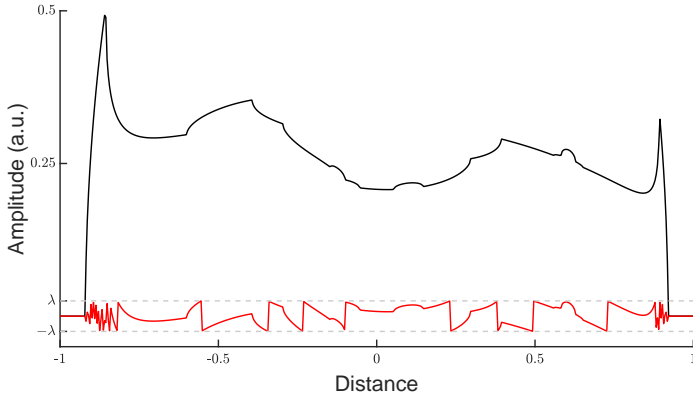


Fig. 2. $\mathcal{R}_\theta f_{\text{SL}}$ (black) and $\mathcal{R}_\theta^\lambda f_{\text{SL}}$ (red) for $\theta = \frac{\pi}{2}$ and $\lambda = 0.025$.

III. MODULO RADON TRANSFORM

As mentioned before, to overcome the dynamic range limitation, we propose a generalization of the Radon transform, which we call Modulo Radon Transform and makes use of a modulo operation to enforce projection data with values in the range $[-\lambda, \lambda]$ for a given threshold $\lambda > 0$. To this end, we define the centered modulo operator $\mathcal{M}_\lambda : \mathbb{R} \rightarrow [-\lambda, \lambda]$ with

$$\mathcal{M}_\lambda(t) = 2\lambda \left(\left\lfloor \frac{t}{2\lambda} + \frac{1}{2} \right\rfloor - \frac{1}{2} \right),$$

where $\lfloor t \rfloor = t - [t]$ denotes the fractional part of t . With this, we define the Modulo Radon Transform \mathcal{R}^λ on $\mathbb{S}^1 \times \mathbb{R}$ as

$$\mathcal{R}^\lambda f(\theta, t) = \mathcal{M}_\lambda(\mathcal{R}f(\theta, t)).$$

As before, for fixed angle $\theta \in [0, 2\pi)$ we set

$$\mathcal{R}_\theta^\lambda f = \mathcal{R}^\lambda f(\theta, \cdot) = \mathcal{M}_\lambda(\mathcal{R}_\theta f).$$

As an example, Fig. 1(a) shows the so called Shepp-Logan phantom f_{SL} which is a classical test case in medical imaging. The amplitude is normalized so that $\|f_{\text{SL}}\|_\infty = 1$. In Fig. 1(b), we show the Radon Transform $\mathcal{R}f_{\text{SL}}$ along with the Modulo Radon Transform $\mathcal{R}^\lambda f_{\text{SL}}$ with threshold $\lambda = 0.025$ in Fig. 1(c). In this illustration, the MRT is able to compress the dynamic range $\rho_{f_{\text{SL}}, \lambda} = \|\mathcal{R}_\theta f_{\text{SL}}\|_\infty / 2\lambda$ by about 10 times.

For a better illustration of the modulo operation, Fig. 2 shows the univariate functions $\mathcal{R}_\theta f_{\text{SL}}$ and $\mathcal{R}_\theta^\lambda f_{\text{SL}}$ for fixed projection angle $\theta = \pi/2$ and with threshold $\lambda = 0.025$.

A. The Modulo Radon Transform is Injective

The MRT defines a non-linear operator $\mathcal{R}^\lambda : L^1(\mathbb{R}^2) \rightarrow L^1(\mathbb{S}^1 \times \mathbb{R})$ that might not be injective, since adding multiples of λ does not change the image of \mathcal{M}_λ . However, we now show its injectivity for the band-limited class. This assumption is motivated by the fact that the approximate FBP reconstruction formula (2) is still one of the most applied reconstruction techniques in tomography [22], where the reconstruction filter satisfies

$$\mathcal{F}_1 F_\Omega(S) = |S| W(S/\Omega) \quad (4)$$

with an even window $W \in L^\infty(\mathbb{R})$ supported in $[-1, 1]$, and

$$\mathcal{F}_2 f_\Omega(\mathbf{x}) = W(\|\mathbf{x}\|_2/\Omega) \mathcal{F}_2 f(\mathbf{x}).$$

Hence, (2) provides a band-limited approximation f_Ω to the target function $f \in L^1(\mathbb{R}^2)$, i.e.

$$f_\Omega \in \mathcal{B}_\Omega(\mathbb{R}^2) \iff \mathcal{F}_2 f_\Omega = \mathbb{1}_{B_\Omega(0)} \mathcal{F}_2 f_\Omega,$$

where $\mathbb{1}_{B_\Omega(0)}$ denotes the indicator function of the ball $B_\Omega(0)$.

From now on let f belong to the Bernstein space $\mathcal{B}_\Omega^1(\mathbb{R}^2)$, that is $f \in \mathcal{B}_\Omega^1(\mathbb{R}^2) \iff f \in L^1(\mathbb{R}^2) \cap \mathcal{B}_\Omega(\mathbb{R}^2)$. Thus, applying the Fourier slice theorem (1) shows that we have $\mathcal{R}_\theta f \in \mathcal{B}_\Omega^1(\mathbb{R}) \subset \text{PW}_\Omega$ for all $\theta \in [0, 2\pi)$. Moreover, a direct consequence of [23, Theorem 3] is the injectivity of the modulo operator \mathcal{M}_λ on the Paley-Wiener space PW_Ω .

Lemma 1 (Injectivity of \mathcal{M}_λ). *Any $\phi \in \text{PW}_\Omega$ is uniquely determined by its modulo folded version $\mathcal{M}_\lambda \phi$.*

Consequently, with the injectivity of the Radon Transform follows that

$$\mathcal{R}^\lambda f = \mathcal{R}^\lambda g \implies f = g$$

for all $f, g \in \mathcal{B}_\Omega^1(\mathbb{R}^2)$ and we have shown the following *Injectivity Theorem for Modulo Radon Transform*.

Theorem 1 (Injectivity of the Modulo Radon Transform). *For any threshold $\lambda > 0$ the Modulo Radon Transform \mathcal{R}^λ is injective on the Bernstein space $\mathcal{B}_\Omega^1(\mathbb{R}^2)$ for any $\Omega > 0$.*

In particular, Theorem 1 implies that the MRT is invertible as a mapping $\mathcal{R}^\lambda : \mathcal{B}_\Omega^1(\mathbb{R}^2) \rightarrow \mathcal{R}^\lambda(\mathcal{B}_\Omega^1(\mathbb{R}^2))$.

In the following we demonstrate how to recover f from discrete measurements of its Modulo Radon Transform by applying Unlimited Sampling (US), which has been introduced in [14] and makes use of the forward difference operator Δ as well as the anti-difference operator S . For details on US, we refer to [14], [15].

IV. RECOVERY VIA UNLIMITED SAMPLING

Case 1: Band-limited target function. Let $f \in \mathcal{B}_\Omega^1(\mathbb{R}^2)$ so that $\mathcal{R}_\theta f \in \text{PW}_\Omega$ for all $\theta \in [0, \pi)$. Due to the Unlimited Sampling Theorem [15, Theorem 3], $\mathcal{R}_\theta f$ can be recovered by unlimited sampling from discrete modulo samples $y_\theta^\lambda[m] = \mathcal{R}_\theta^\lambda f(mT)$, $m \in \mathbb{Z}$, if the sampling rate satisfies $T \leq 1/2\Omega e$. The recovery procedure is outlined in Algorithm 1. Consequently, $\mathcal{R}f$ can be recovered by unlimited sampling from semi-discrete MRT samples

$$\{\mathcal{R}_\theta^\lambda f(mT) \mid \theta \in [0, \pi), m \in \mathbb{Z}\}.$$

Since $\mathcal{R}_\theta f \in \text{PW}_\Omega$, the approximate FBP reconstruction formula (2) uniquely recovers f from $\mathcal{R}f$ if the Ram-Lak filter is used, which satisfies $\mathcal{F}_1 F_\Omega(S) = |S| \mathbb{1}_{[-\Omega, \Omega]}(S)$.

Theorem 2. *Any $f \in \mathcal{B}_\Omega^1(\mathbb{R}^2)$ can be recovered from MRT samples $\{\mathcal{R}^\lambda f(\theta, mT) \mid \theta \in [0, \pi), m \in \mathbb{Z}\}$ if $T \leq 1/2\Omega e$.*

Case 2: Arbitrary target function. In case of $f \in L^1(\mathbb{R}^2)$ we perform the following steps:

- (i) For fixed $\theta \in [0, \pi)$ we start with pre-filtering $\mathcal{R}_\theta f$ with the ideal low-pass filter $\Phi_\Omega \in \text{PW}_\Omega$. The resulting band-limited Radon Projection (cf. (3)) takes the form

$$p_\theta(t) = \int_{\mathbb{R}} \mathcal{R}_\theta f(S) \Phi_\Omega(t - S) dS.$$

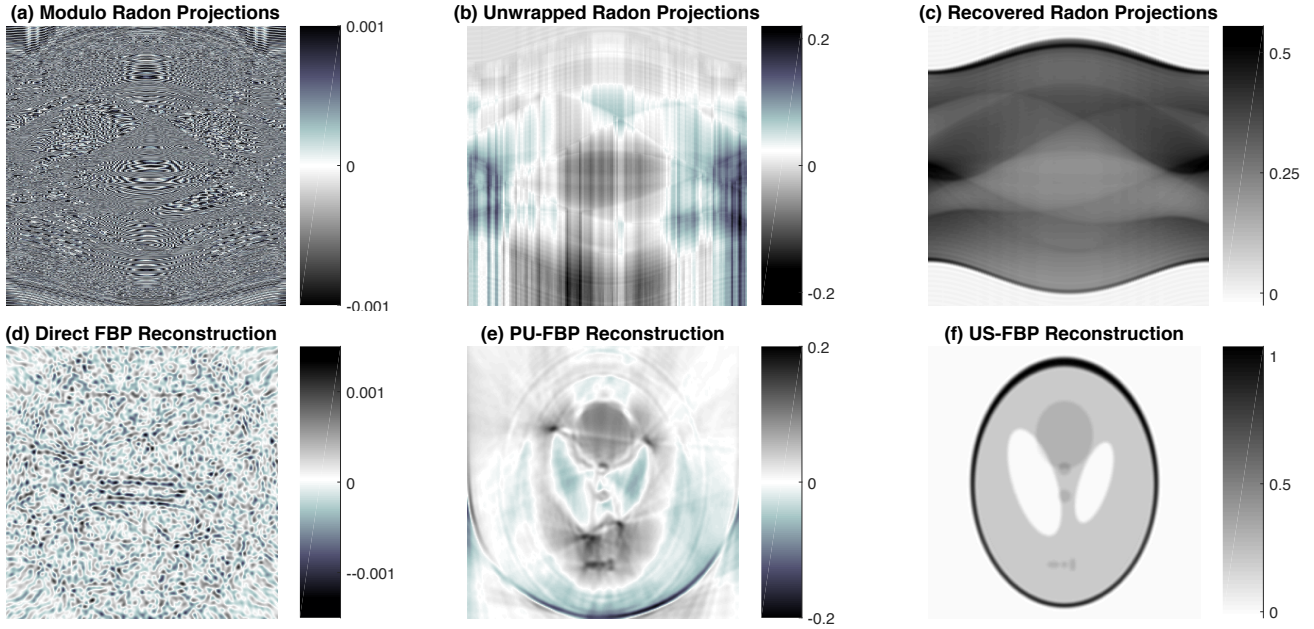


Fig. 3. Demonstration of US-FBP reconstruction for the Shepp-Logan phantom. (a) MRT projections. (b) Recovery using phase unwrapping. (c) Recovery using proposed method. (d) FBP on Modulo Radon data in (a). (e) FBP on unwrapped Radon data in (b). (f) FBP on recovered Radon data in (c).

- (ii) The Radon Projection p_θ is folded in the range $[-\lambda, \lambda]$ via modulo operator \mathcal{M}_λ resulting in the Modulo Radon Projection $p_\theta^\lambda(t) = \mathcal{M}_\lambda(p_\theta(t))$.
- (iii) The Modulo Radon Projection p_θ^λ is sampled with rate T yielding $p_\theta^\lambda[m] = p_\theta^\lambda(mT) = \mathcal{M}_\lambda(p_\theta(mT))$ for $k \in \mathbb{Z}$.

By construction we have $p_\theta \in \text{PW}_\Omega$ for all $\theta \in [0, \pi)$. Due to [15, Theorem 3], p_θ can be recovered by unlimited sampling from discrete modulo samples $p_\theta^\lambda[m] = p_\theta^\lambda(mT)$, $m \in \mathbb{Z}$, if the sampling rate satisfies $T \leq 1/2\Omega e$. Following this, we apply the approximate FBP reconstruction formula (2) to the recovered Radon Projections $p_\theta = \mathcal{R}f * \Phi_\Omega$ yielding the so called *US-FBP reconstruction* denoted by f_Ω^λ .

Algorithm 1 Unlimited Sampling-Filtered Back Projection

Input: samples $y_\theta^\lambda[k] = \mathcal{R}_\theta^\lambda f(kT)$ for $k \in \mathbb{Z}$ and $\theta \in [0, \pi)$, upper bound $2\lambda\mathbb{Z} \ni \beta_f \geq \|f\|_\infty$

- 1: **choose** $N = \left\lceil \frac{\log(\lambda) - \log(\beta_f)}{\log(T\Omega e)} \right\rceil$, $J = 6 \frac{\beta_f}{\lambda}$
- 2: $s_{(0)}[k] = (\mathcal{M}_\lambda(\Delta^N y_\theta^\lambda) - \Delta^N y_\theta^\lambda)[k]$
- 3: **for** $n = 0, \dots, N - 2$ **do**
- 4: $s_{(n+1)}[k] = 2\lambda \left\lceil \frac{\lfloor S_{s_{(n)}}[k]/\lambda \rfloor}{2} \right\rceil$
- 5: $\kappa_n = \left\lceil \frac{s_{(n+1)}[1] - s_{(n+1)}[J+1]}{12\beta_f} + \frac{1}{2} \right\rceil$
- 6: $s_{(n+1)}[k] = s_{(n+1)}[k] + 2\lambda\kappa_n$
- 7: **end for**
- 8: $y_\theta[k] = y_\theta^\lambda[k] + (S_{s_{(N-1)}})[k]$

$$9: \mathcal{R}_\theta f = \sum_{k \in \mathbb{Z}} y_\theta[k] \text{sinc}\left(\frac{\pi}{T}(\cdot - kT)\right)$$

Output: US-FBP reconstruction $f_\Omega^\lambda = \frac{1}{2} \mathcal{R}^\#(F_\Omega * \mathcal{R}_\theta f)$

A Note on US-FBP Error Bound. If we use a reconstruction filter F_Ω satisfying (4), we observe that

$$f_\Omega = \frac{1}{2} \mathcal{R}^\#(F_\Omega * \mathcal{R}_\theta f) = \frac{1}{2} \mathcal{R}^\#(F_\Omega * p_\theta)$$

and, thus, existing error estimates for the FBP approximation error $f - f_\Omega$ carry over to the US-FBP error $f - f_\Omega^\lambda$. To illustrate this, we apply [19, Theorem 5.5] and [20, Theorem 3] to obtain error estimates in Sobolev spaces of fractional order $\alpha > 0$, given by $H^\alpha(\mathbb{R}^2) = \{f \in L^2(\mathbb{R}^2) \mid \|f\|_\alpha < \infty\}$, where

$$\|f\|_\alpha^2 = \frac{1}{4\pi^2} \int_{\mathbb{R}^2} (1 + \|\mathbf{x}\|_2^2)^\alpha |\mathcal{F}_2 f(\mathbf{x})|^2 d\mathbf{x}.$$

Theorem 3 (Reconstruction Error Bound). For $\alpha > 0$, let $f \in L^1(\mathbb{R}^2) \cap H^\alpha(\mathbb{R}^2)$ and, for $\lambda > 0$, let f_Ω^λ denote the US-FBP reconstruction from semi-discrete Modulo Radon Projections $\{p_\theta^\lambda(mT) \mid \theta \in [0, \pi), m \in \mathbb{Z}\}$ with $T \leq 1/2\Omega e$. If the reconstruction filter's window satisfies $W \in \mathcal{C}[-1, 1]$ and $W(S) = 1$ for $S \in [-c_W, c_W]$ with $c_W > 0$, then the L^2 -norm of the US-FBP error is bounded above by

$$\|f - f_\Omega^\lambda\|_{L^2(\mathbb{R}^2)} \leq (c_W^{-\alpha} \|1 - W\|_\infty + 1) \Omega^{-\alpha} \|f\|_\alpha.$$

Alternatively, if $W \in \mathcal{C}^{k-1, \nu}[-1, 1]$ for $k \in \mathbb{N}$, $\nu \in (0, 1]$ and $W(0) = 1$, $W^{(j)}(0) = 0 \forall 1 \leq j \leq k-1$, then the L^2 -norm of the US-FBP error is bounded by

$$\|f - f_\Omega^\lambda\|_{L^2(\mathbb{R}^2)} \leq c_{\alpha, W} \Omega^{-\min\{k-1, \nu, \alpha\}} \|f\|_\alpha$$

with an explicitly known constant $c_{\alpha, W} > 0$.

V. NUMERICAL EXPERIMENTS

In our numerical experiments we use the proposed US-FBP framework to recover the Shepp-Logan phantom on a grid of 256×256 pixels from finitely many Modulo Radon Projections

$$\{p_{\theta_k}^\lambda(t_m) \mid -M \leq m \leq M, 0 \leq k \leq K-1\}$$

in parallel beam geometry with $t_m = mT$ and $\theta_k = k \frac{\pi}{K}$. To this end, the FBP formula (2) is discretized using a standard approach and according to [24, Section 5.1.1], the optimal sampling conditions are given by $T \leq \pi/\Omega$, $M \geq 1/T$, $K \geq \Omega$.

The results are summarized in Fig. 3, where we used the bandwidth $\Omega = 180$, threshold $\lambda = 0.001$, the parameters $T = 1/2\Omega e$, $M = \lceil 1/T \rceil$, $K = \Omega$, and the cosine filter with $\mathcal{F}_1 F_\Omega(S) = |S| \cos\left(\frac{\pi S}{2\Omega}\right) \mathbb{1}_{[-\Omega, \Omega]}(S)$. As predicted by our theory, the FBP reconstruction from conventional Radon Transform data and the US-FBP reconstruction from Modulo Radon Projections yield approximately the same root mean square error (RMSE) of 7.229×10^{-2} .

Remarks on Numerical Assessment. For comparison, we also applied Phase Unwrapping (PU) in place of Unlimited Sampling for recovering Radon Projections from Modulo Radon Projections. The result is displayed in Fig. 3(b) and the corresponding FBP reconstruction fails, as shown in Fig. 3(e). When λ is small, higher order differences are needed for recovery. This can be tackled by the Unlimited Sampling approach but is a fundamental limitation of the PU method which only works for single order difference [15].

Secondly, we note that empirically the US-FBP method works with a much slower sampling rate T so that the condition $T \leq (2\Omega e)^{-1}$ is *not* fulfilled. Note that the choice $T = 1/(2\Omega e)$ corresponds to an oversampling factor of $2\pi e$ compared to the Nyquist rate. In our numerical experiments with the Shepp-Logan phantom and $\lambda = 0.001$ we found that the reconstruction succeeds even for $T = \pi/(4\Omega)$, which corresponds to a much smaller oversampling factor of 4.

Finally, we remark that the proposed US-FBP method is *empirically stable* in the presence of noise in the modulo samples. To demonstrate this, we added white Gaussian noise with SNR of 32.5 dB to the Modulo Radon Projections of the Shepp-Logan phantom with $\lambda = 0.05$, which leads to an RMSE of 6.4×10^{-4} . Unlimited Sampling succeeds to recover the Radon Projections up to the same RMSE and the error between the US-FBP reconstruction and the FBP reconstruction from conventional Radon data is 3.3×10^{-4} .

VI. CONCLUSIONS

In this work, we propose the Modulo Radon Transform (MRT) which is obtained from the modulo of line integrals used in the usual Radon Transform. We discuss conditions under which the MRT is an injective mapping and complement our approach with an inversion method. Recent advances in the tomography source technologies require modifications to both hardware and algorithms so that high dynamic range (HDR) reconstructions are possible. As an alternative to existing multiple-exposure HDR tomography, the MRT allows for

single-shot reconstruction. Beyond tomography, in the general context of Radon Transform our work leads to a new class of inverse problems with several interesting future directions. For instance, a Fourier Slice Projection theorem for the MRT would strengthen the applicability of our approach.

REFERENCES

- [1] P. Funk, "Über eine geometrische Anwendung der abelschen Integralgleichung", *Mathematische Annalen*, vol. 77, no. 1, pp. 129–135, 1915.
- [2] J. Radon, "Über die Bestimmung von Funktionen durch ihre Integralwerte längs gewisser Mannigfaltigkeiten", *Ber. Sächs. Akad. Wiss.*, vol. 69, pp. 262–277, 1917.
- [3] A. M. Cormack, "Representation of a function by its line integrals, with some radiological applications", *Journal of Applied Physics*, vol. 34, no. 9, pp. 2722–2727, 1963.
- [4] D. Ludwig, "The Radon transform on Euclidean space", *Communications on Pure and Applied Mathematics*, vol. 19, no. 1, pp. 49–81, 1966.
- [5] P. Rattey and A. Lindgren, "Sampling the 2-d Radon transform", *IEEE Trans. Acoust., Speech, Signal Process.*, vol. 29, no. 5, pp. 994–1002, 1981.
- [6] W. H. Press, "Discrete Radon transform has an exact, fast inverse and generalizes to operations other than sums along lines", *Proceedings of the National Academy of Sciences*, vol. 103, no. 51, pp. 19249–19254, 2006.
- [7] O. Tretiak and C. Metz, "The exponential Radon transform", *SIAM Journal on Applied Mathematics*, vol. 39, no. 2, pp. 341–354, 1980.
- [8] P. Chen, Y. Han, and J. Pan, "High-dynamic-range CT reconstruction based on varying tube-voltage imaging", *PLOS ONE*, vol. 10, no. 11, p. e0141789, 2015.
- [9] Y. Li, Y. Han, and P. Chen, "X-ray energy self-adaption high dynamic range (HDR) imaging based on linear constraints with variable energy", *IEEE Photon. J.*, vol. 10, no. 1, p. 3400114, 2018.
- [10] P. Eppenberger, M. Marcon, M. Ho, F. D. Grande, T. Frauenfelder, and G. Andreisek, "Application of a colored multiexposure high dynamic range technique to radiographic imaging", *Journal of Computer Assisted Tomography*, vol. 40, no. 4, pp. 658–662, 2016.
- [11] C. Vinegoni, C. L. Swisher, P. F. Feruglio, R. J. Giedt, D. L. Rousso, S. Stapleton, and R. Weissleder, "Real-time high dynamic range laser scanning microscopy", *Nature Communications*, vol. 7, no. 1, 2016.
- [12] A. Degirmenci, D. P. Perrin, and R. D. Howe, "High dynamic range ultrasound imaging", *International Journal of Computer Assisted Radiology and Surgery*, vol. 13, no. 5, pp. 721–729, 2018.
- [13] J. T. Weiss, K. S. Shanks, H. T. Philipp, J. Becker, D. Chamberlain, P. Purohit, M. W. Tate, and S. M. Gruner, "High dynamic range x-ray detector pixel architectures utilizing charge removal", *IEEE Trans. Nucl. Sci.*, vol. 64, no. 4, pp. 1101–1107, 2017.
- [14] A. Bhandari, F. Kraemer, and R. Raskar, "On unlimited sampling", in *Intl. Conf. on Sampling Theory and Applications (SampTA)*, pp. 31–35, 2017.
- [15] —, "On unlimited sampling and reconstruction", arXiv:1905.03901, 2019.
- [16] —, "Methods and apparatus for modulo sampling and recovery," U.S. Patent (US 10651865 B2), May 2020.
- [17] A. Arbel and R. Kurz, "Fast ADC", *IEEE Trans. Nucl. Sci.*, vol. 22, no. 1, pp. 446–451, 1975.
- [18] J. Rhee and Y. Joo, "Wide dynamic range CMOS image sensor with pixel level ADC", *Electron. Lett.*, vol. 39, no. 4, p. 360, 2003.
- [19] M. Beckmann and A. Iske, "Error Estimates and Convergence Rates for Filtered Back Projection", *Math. Comp.*, vol. 88, no. 316, pp. 801–835, 2019.
- [20] —, "Convergence Rates for Hölder-Windows in Filtered Back Projection", in *Intl. Conf. on Sampling Theory and Applications (SampTA)*, 2019.
- [21] —, "Saturation Rates of Filtered Back Projection Approximations", *Calcolo*, vol. 57, no. 1, 12, 2020.
- [22] X. Pan, E. Sidky, and M. Vannier, "Why do commercial CT scanners still employ traditional, filtered back-projection for image reconstruction?", *Inverse Problems*, vol. 25, no. 12, p. 123009, 2009.
- [23] A. Bhandari and F. Kraemer, "On identifiability in unlimited sampling", in *Intl. Conf. on Sampling Theory and Applications (SampTA)*, 2019.
- [24] F. Natterer and F. Wübbeling, "Mathematical Methods in Image Reconstruction", SIAM, Philadelphia, 2001.